frontiers in Water

ORIGINAL RESEARCH
published: 08 December 2020
doi: 10.3389/frwa.2020.577511

Hydrogeochemical Dynamics and Response of Karst Catchment to Rainstorms in a Critical Zone Observatory (CZO), Southwest China

Caiqing Qin[1,2], *Hu Ding*[1]*, *Si-Liang Li*[1,3,4], *Fu-Jun Yue*[1], *Zhong-Jun Wang*[5] and *Jie Zeng*[6]

[1] *Institute of Surface-Earth System Science, School of Earth System Science, Tianjin University, Tianjin, China,* [2] *Department of Earth & Environmental Science, School of Human Settlements and Civil Engineering, Xi'an Jiaotong University, Xi'an, China,* [3] *State Key Laboratory of Environmental Geochemistry, Institute of Geochemistry, Chinese Academy of Sciences, Guiyang, China,* [4] *Puding Karst Ecosystem Observation and Research Station, Chinese Academy of Sciences, Puding, China,* [5] *Department of Water Environment, China Institute of Water Resources and Hydropower Research, Beijing, China,* [6] *Institute of Earth Sciences, China University of Geosciences (Beijing), Beijing, China*

OPEN ACCESS

Edited by:
Carl I. Steefel, Lawrence Berkeley National Laboratory, United States

Reviewed by:
Kalyana Babu Nakshatrala, University of Houston, United States
Reza Soltanian, University of Cincinnati, United States

***Correspondence:**
Hu Ding
dinghu@tju.edu.cn

Specialty section:
This article was submitted to Water and Critical Zone, a section of the journal Frontiers in Water

Received: *29 June 2020*
Accepted: *23 October 2020*
Published: *08 December 2020*

Citation:
Qin C, Ding H, Li S-L, Yue F-J, Wang Z-J and Zeng J (2020) Hydrogeochemical Dynamics and Response of Karst Catchment to Rainstorms in a Critical Zone Observatory (CZO), Southwest China. Front. Water 2:577511. doi: 10.3389/frwa.2020.577511

Karst water is vital for local drinking and irrigation but is susceptible to contamination. Hydrochemistry, which is highly related to carbonate weathering in karst catchments, can affect water quality and respond rapidly to climate change. In order to explore hydrogeochemical sources, dynamics, and their responses to rainstorms, rainwater, throughfall, hillslope runoff, surface water, and groundwater were sampled synchronously during rainstorms at a karst Critical Zone Observatory (CZO), Southwest China. Results showed that the total dissolved solids (TDS) concentration in throughfall increased by 30.1 ± 8.0% relative to rainwater, but both throughfall and rainwater contributed little to TDS in surface water and groundwater compared with terrestrial sources. Hydrochemistry in surface water and groundwater was diluted by rainstorms but displayed chemostatic responses with different intensities to increasing discharge. This is possibly regulated by hydrogeological conditions, available sources of various solutes, and the difference between solute concentrations before and after rainstorms. Ca^{2+} and Mg^{2+} dynamics were mainly regulated by carbonate weathering, gypsum dissolution, and gypsum-induced dedolomitization (geological sources), which also affect Ca^{2+}, Mg^{2+}, and SO_4^{2-} in deep confined groundwater draining a gypsum stratum. For HCO_3^-, CO_2 from respiration and microbiologic activities is one dominant contributor, especially for spring. The chemostatic behaviors of NO_3^-, Cl^-, and K^+ were related to agricultural activities, especially in surface water. These controls on hydrochemistry may already exist as hillslope runoff occurs, which has be further demonstrated by principle component analysis (PCA). The heterogeneous permeability of epikarst can affect the mixture of groundwater from different sources and flowing pathways, enabling hydrochemistry at different hydrogeological conditions to display discrepant responses to rainstorms. The epikarst aquifer with high permeability is susceptible to changes in external environment,

such as rainstorms and agricultural activities, increasing the potential risk of water environment problems (chronic pollution of nitrogen and high hardness of water) during a certain period. Drinking water safety thus deserves consideration in the agricultural karst catchment.

Keywords: hydrochemistry, high-resolution data, rainstorms, chemical weathering, chemostatic behavior, karst catchment

INTRODUCTION

Karst landforms cover 2.2×10^7 km^2 and are scattered around the world, especially in Southeast Asia, South America, and the Mediterranean coasts (Yuan and Cai, 1988; Ford and Williams, 2007). Southeast Asia is the largest continuous karst region, centered on Southwest China (Zhao and Seip, 1991). Comprised of chemically soluble rocks with large passages or network of conduits and caves inside, karst aquifers are very permeable and can store and transport large amounts of water, supplying drinking and irrigation water to ∼25% of the world's population (Ford and Williams, 2007). However, the increasing water demand (residential, industrial, and agricultural use) can cause water shortage and water quality degradation. Additionally, the special hydrogeological conditions (high permeable soil/rock systems with caves and fractures inside) of karst systems benefit water and solutes migration, making the CO_2-H_2O-$CaCO_3$ system sensitive to hydrological changes (Yuan and Zhang, 2008; Beaulieu et al., 2012), and making karst aquifers vulnerable to contamination (Kačaroglu, 1999). Researching karstic hydrochemical dynamics during rainfall storms is conducive to understanding the transfer of contaminants and solutes and their responses to climate change.

Intense carbonate weathering and mixing of "new" and "old" water can alter solute concentrations in karst water (Gabet et al., 2006; Basu et al., 2010). Solute concentrations also normally show distinct seasonal patterns due to hydrological variations and some biogeochemical processes (Han and Liu, 2004; Lang et al., 2006; Zhong et al., 2020). Therefore, hydrogeochemical behaviors in karst catchments need to be demonstrated by high-resolution information that can capture key processes. High-frequency field campaigns during rainstorms are thus necessary to analyze the dynamic response of chemical compositions to hydrological variations and its potential effects on water quality as well as public health. The dynamic behaviors and corresponding controls of hydrochemistry in river and/or groundwater have been reported (Koger et al., 2018; Piazza et al., 2018; Correa et al., 2019). However, there are few studies conducting high-frequency sampling to analyze hydrochemistry in both surface water and groundwater in karst regions of Southwest China. Additionally, rainwater, one important source of surface and ground water, also plays a significant role in hydrochemical dynamics (Polkowska et al., 2005; Ma et al., 2017). But most research only pays attention to sources of solutes in rainwater (Han and Liu, 2006; Lu et al., 2011; Wu et al., 2012; Zhang et al., 2012; Rao et al., 2017; Zhou et al., 2019); the dynamic variation of hydrochemistry among different waters (rainwater, throughfall, hillslope runoff, surface water, and groundwater) are rarely explored during rainstorms. Rainwater may play a more important role in karst catchments than non-karst systems, since the acidic rainwater may also dissolve carbonate minerals and then alter the hydrochemistry as well. Analyzing hydrochemistry of different water bodies in spatial profile can offer comprehensive information to understand hydrogeochemical dynamics in Earth's Critical Zone. This is necessary for modeling the migration processes of hydrochemistry and better implementing cost-effective water quality management in karst catchment.

Against this background, high-frequency sampling for surface water and spring was conducted during rainstorms at a karst catchment in Southwest China. Rainwater, throughfall, hillslope runoff, and well water were also synchronously collected, to analyze (1) the dynamic response of surface water and groundwater to rainstorms and corresponding controls and (2) the dynamic variations of hydrochemistry among different water bodies at a catchment scale and corresponding controls.

MATERIALS AND METHODS

Study Area

Chenqi catchment (26°15′20″-26°16′9″N, 105°46′3″-105°46′50″E), with an area of 1.25 km^2, is a karst Critical Zone Observatory (CZO) located in Puding, Guizhou province, Southwest China (**Figure 1**). This CZO has been investigated for ∼40 years in the aspect of hydrogeological structure, hydrological connectivity, soil characteristics, and other fundamental information (Chen et al., 2005, 2018; Cheng et al., 2019; Zhang et al., 2019; Liu M. et al., 2020). It is an agricultural karst catchment where irrigation and drinking water are both supplied by karst water. Under the influence of a subtropical monsoonal climate, the annual mean rainfall is 1,140 mm, over 80% of which falls in the wet season. Average monthly air temperature is highest in August (24°C) but lowest in December (7°C). Average monthly humidity ranges from 74 to 78%.

The elevation of this catchment decreases from east of 1,520 m to west of 1,320 m (outlet). Carbonate rocks dominate the lithology, over which Quaternary soils are unevenly distributed. Limestone is the dominant geological strata in the higher elevation area with 150–200 m thickness, and the underlying layer is impermeable marlite strata (Zhang et al., 2019). Soil is thin (mean < 50 cm) in hills but thicker (40–100 cm) in valley depressions. Deciduous broad-leaved forest and scrub-grassland, occupying 83% of total land use, grow mainly on the mountains. Agricultural paddy and dry land are spread in valley depressions, accounting for about 3 and 14% of the catchment area, respectively (Qin et al., 2020). The catchment outlet is in the valley depression surrounded by scattered hills. There are three

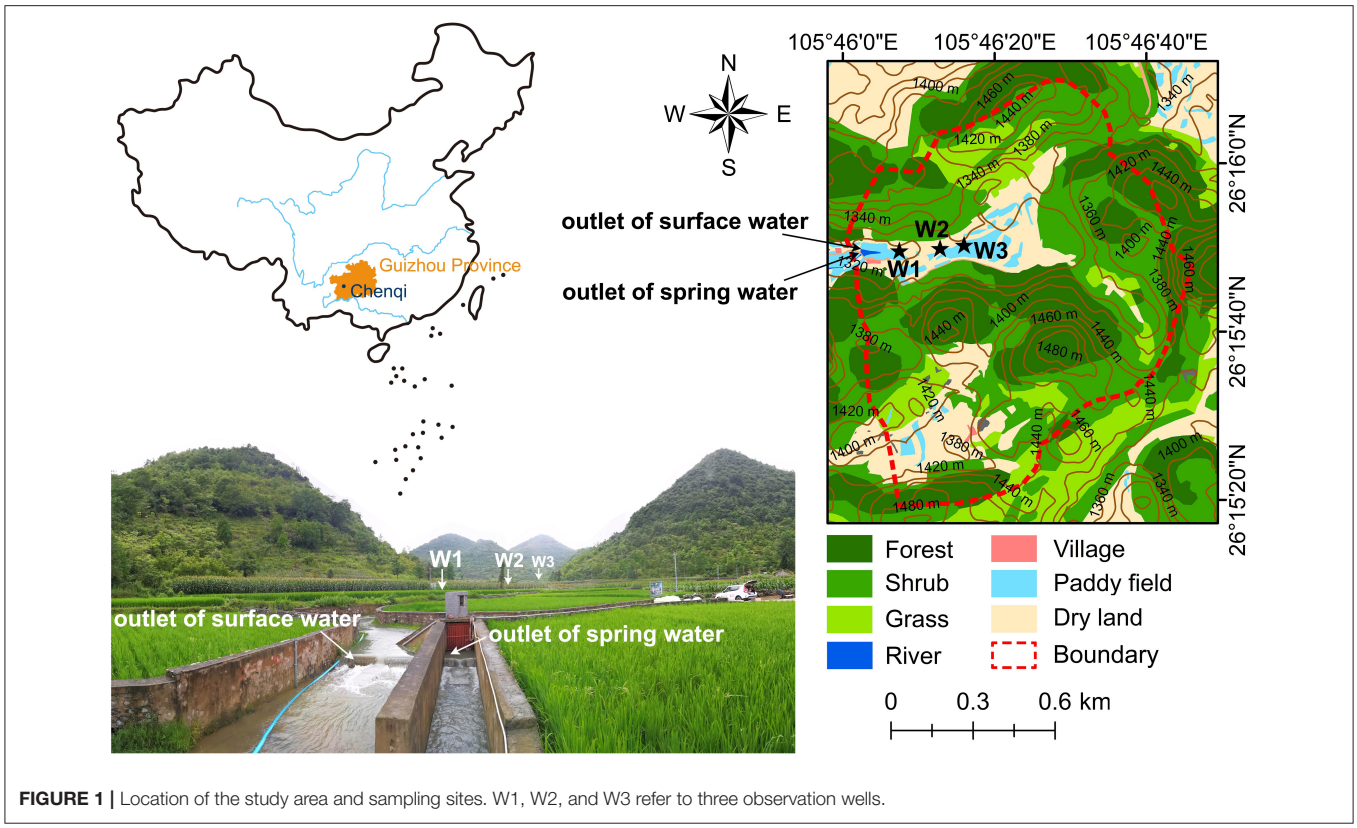

FIGURE 1 | Location of the study area and sampling sites. W1, W2, and W3 refer to three observation wells.

observation wells with different depth distributed in depression (**Figure 1**). The depth (below the ground surface) of well W1 and well W3 are 20 and 12 m, respectively. The permeability of aquifer around W1 is low (most resistivity > 1,000 Ωm) but that around W3 is high (most resistivity < 100 Ωm) (Chen et al., 2018). The well W2 (depth > 20 m) is fed by deep confined spring draining gypsum stratum and scarcely suffers outside disturbance. The 3-wells can thus reflect the circumstances at different depth in the karst structure.

Sampling and Measurement

High-frequency sampling was conducted at the outlet of spring (SP) and surface water (SU) during rainstorms from June 11 to 17, 2018 (**Figure 1**). Well water samples of W2 were synchronously collected at the outlet through a drain line. Well water at different depths of W1 and W3 were sampled before (B), during (D), after (A) and on the fourth days (F) after the rainstorms. Meanwhile, rainwater (RA), throughfall (TH), and hillslope runoff (HI) were also collected on surrounding hills.

At the sampling time, water temperature (T), dissolved oxygen (DO), electrical conductivity (EC), and pH were measured in the field by a portable multiple parameter sensor (WTW, Multi 3630 IDS). All water samples were collected in duplicate in dry and clean bottles that were rinsed twice beforehand with *in-situ* water and stored in darkness at 4°C until analysis. One part was used for measuring HCO_3^- concentration through acid titration with 0.02 mol L^{-1} HCl. The other was filtered through 0.22 μm filters to measure major ions (Ca^{2+}, Mg^{2+}, Na^+, K^+, SO_4^{2-}, Cl^-, NO_3^-) by the Ion Chromatography (Thermo Scientific, Dionex Aquion). Blank test and sample duplicates were conducted during analytical processes to perform quality assurance and control. The blank was lower than the method detection limits and the relative standard deviation (RSD) of above analyses were all within 5%.

Total dissolved solids (TDS) were calculated by the sum of eight ions measured above. The bracket "[]" was used to symbolize the concentration of solutes, e.g., Ca^{2+} concentration is simply described as $[Ca^{2+}]$. To more accurately compare solute concentrations within this study or between different researches, discharge-weighted concentration (DWC) of solutes was calculated as follows:

$$DWC = \frac{\sum (Q_i \times C_i)}{\sum Q_i} \quad (1)$$

where Q_i is the discharge at timestep i and C_i is the synchronous concentration of solutes.

RESULTS

During the sampling period, two considerable rainstorms occurred continuously, with amounts of 30.4 mm on June 11 and 24 mm on June 12 (**Figure 2**). The pH value of rainwater here is 6.27 ± 0.03, which increases by 0.44 in throughfall (**Supplementary Table 1**). Ion concentrations in rainwater are low and follow the order of $[HCO_3^-]$ (109 μmol L^{-1}) > $[SO_4^{2-}]$

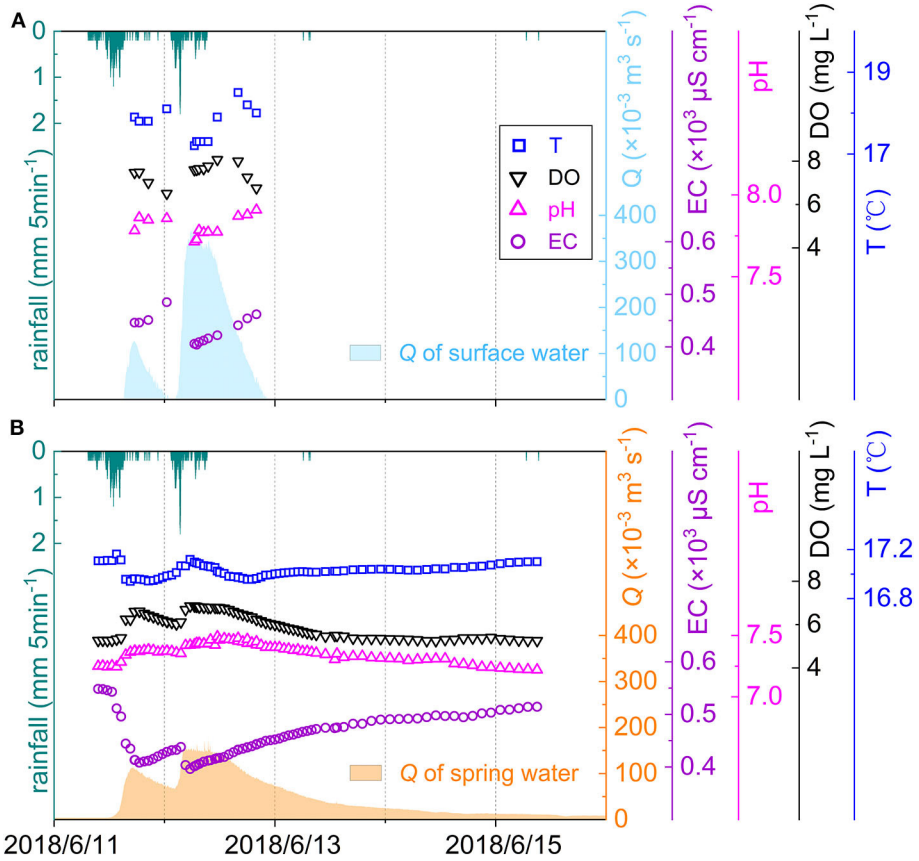

FIGURE 2 | Time series of rainfall, discharge (Q), and water quality parameters of surface water **(A)** and spring water **(B)**.

(79.8 μmol L^{-1}) > [Ca^{2+}] (46.3 μmol L^{-1}) > [NO_3^-] (30.7 μmol L^{-1}) > [Mg^{2+}] (7.87 μmol L^{-1}) > [K^+] (3.57 μmol L^{-1}) > [Na^+] (2.76 μmol L^{-1}) > [Cl^-] (2.40 μmol L^{-1}) (**Supplementary Table 1**). The first four ions dominate chemical compositions, accounting for 94.1%. After passing through the vegetation canopy, [NO_3^-] decreases by 9.13 ± 6.13 μmol L^{-1} but other ions increase with different degrees. The TDS concentration in TH is slightly higher than that in RA (24.2 vs. 18.6 mg L^{-1}). Both RA and TH show lower total cation charge ($TZ^+ = 2[Ca^{2+}] + 2[Mg^{2+}] + [Na^+] + [K^+]$) than total anion charge ($TZ^- = [HCO_3^-] + 2[SO_4^{2-}] + [NO_3^-] + [Cl^-]$). The net inorganic charge balance (NICB = $[TZ^+ - TZ^-] / [TZ^+ + TZ^-]$ * 100%) in RA is even <-10% (**Figure 3**).

During rainstorms, discharge varied from 0.4 × 10^{-3} to 179.5 × 10^{-3} m^3 s^{-1} at SP outlet and from 0 to 378.1 × 10^{-3} m^3 s^{-1} at SU outlet, and high discharge normally accompanied high DO and low EC (**Figure 2**). SU samples have higher DO and pH but lower EC compared with SP samples, and all of them have small coefficient of variation (CV < 10%) (**Supplementary Table 1**). TDS in SU and SP range from 331 to 397 mg L^{-1} and from 345 to 475 mg L^{-1}, respectively. The DWC of ions in SU follow the order of [HCO_3^-] (3,371 μmol L^{-1}) > [Ca^{2+}] (1,804 μmol L^{-1}) > [Mg^{2+}] (362 μmol L^{-1}) > [SO_4^{2-}] (333 μmol L^{-1}) > [NO_3^-] (321 μmol L^{-1}) > [Cl^-] (73.4 μmol L^{-1}) > [Na^+] (35.5 μmol L^{-1}) > [K^+] (33.5 μmol L^{-1}) (**Supplementary Table 1**). In SP, the DWC of HCO_3^-, Ca^{2+}, and Mg^{2+} are higher than that in SU, at 3,812, 2,053, and 436 μmol L^{-1}, respectively. While the DWC of NO_3^-, Cl^-, and K^+ in SP are lower than that in SU, at 217, 61.0, and 21.8 μmol L^{-1}, respectively. Except NO_3^-, parameters have higher CV in SP than in SU (**Supplementary Table 1**). The NICB of both SU and SP samples are within ±10% (**Figure 3**).

The water levels in W1 and W3 fluctuated by 1.6 and 3.7 m, respectively (**Supplementary Figure 1**). All ion concentrations in W1 have relatively small spatial variations in vertical profiles and temporal variations among the four sampling campaigns [before (B), during (D), after (A), and on the fourth days (F) after the rainstorms], as reflected by their CV in **Supplementary Table 1** and box plots in **Figure 4**. In vertical profiles of W3, however, ion concentrations normally fluctuate more widely, except the third sampling (A) when almost all ions have the minimum CV. The mean ion concentrations in W1 follow the order of [HCO_3^-] (4,434 μmol L^{-1}) > [Ca^{2+}] (2,355 μmol L^{-1}) > [SO_4^{2-}] (1,743 μmol L^{-1}) > [Mg^{2+}] (1,385 μmol L^{-1}) > [Cl^-] (122 μmol L^{-1}) > [K^+] (98.4 μmol L^{-1}) > [Na^+] (68.9 μmol L^{-1}) > [NO_3^-] (64.3 μmol L^{-1}) (**Supplementary Table 1**). In W3, the mean [Ca^{2+}], [Na^+], [NO_3^-], and [Cl^-] are higher, at 2,672, 81.9, 526, and 199 μmol L^{-1}, respectively. But [Mg^{2+}], [HCO_3^-], [SO_4^{2-}], and [K^+] are lower, at 653, 3,819, 1,114, and 33.0 μmol L^{-1},

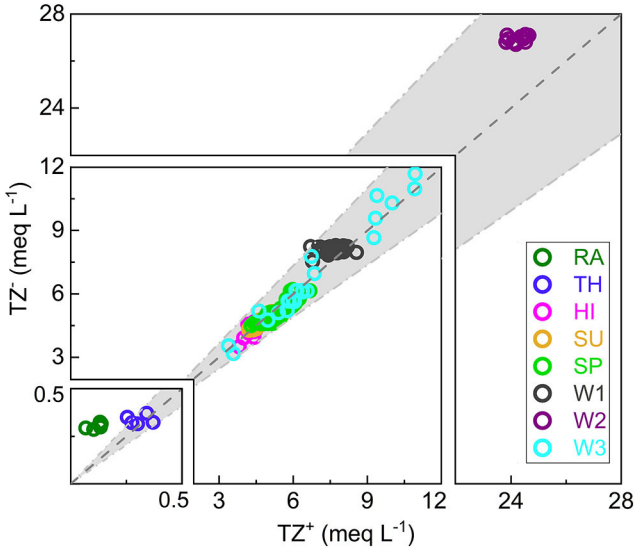

FIGURE 3 | The correlation between total cation charge ($TZ^+ = 2[Ca^{2+}] + 2[Mg^{2+}] + [Na^+] + [K^+]$) and total anion charge ($TZ^- = [HCO_3^-] + 2[SO_4^{2-}] + [NO_3^-] + [Cl^-]$). The light gray zone stands for that the net inorganic charge balance (NICB = $[TZ^+ - TZ^-] * 100/ [TZ^+ + TZ^-]$) is within ±10. RA, TH, HI, SU, and SP refer to rainwater, throughfall, hillslope runoff, surface water, and spring water, respectively. W1, W2, and W3 refer to three observation wells.

respectively. The water velocity of W2 flowing from the drain pipeline was almost unchanged. All ion concentrations in W2 are relatively stable at different depths or moments throughout the whole rainstorms, following the order of $[SO_4^{2-}]$ (11,560 μmol L^{-1}) > $[Ca^{2+}]$ (8,003 μmol L^{-1}) > $[Mg^{2+}]$ (3,952 μmol L^{-1}) > $[HCO_3^-]$ (3,766 μmol L^{-1}) > $[Na^+]$ (262 μmol L^{-1}) > $[K^+]$ (66.4 μmol L^{-1}) > $[Cl^-]$ (39.6 μmol L^{-1}) > $[NO_3^-]$ (10.3 μmol L^{-1}) (**Supplementary Table 1**).

DISCUSSIONS

Dynamic Responses of Surface Water and Groundwater to Rainstorms

Solute concentrations normally vary inversely with discharge, which can be well reflected by power-law function (Godsey et al., 2009; Musolff et al., 2015; Zimmer et al., 2019; Ackerer et al., 2020). To demonstrate relationships between concentrations and discharge, power-law function was adopted as follows:

$$C_i = aQ_i^b \quad (2)$$

where C_i and Q_i are instantaneous solute concentrations (C) and discharge (Q) at timestep i. The exponent "b" is an indicator reflecting the sensitivity of solute concentrations to discharge variation (Godsey et al., 2009). When $b = -1$, solute fluxes (the product of C and Q) equal the constant "a" and the dilution effect occurs; when b is near-zero, chemostatic behavior occurs; when $b > 0$, the flushing effect arises. In this study, the C-Q fitting curves generate "b" closer to 0 for HCO_3^-, Ca^{2+}, and Mg^{2+} than other ions (**Figure 5**), indicating that there are more supplementary inputs alleviating dilution of increasing discharge, resulting in stronger chemostatic response (Clow and Mast, 2010). Except NO_3^- and Na^+, other ions all exhibit weaker chemostatic behavior in SP than SU (**Figure 5**). This observation may be largely related to their initial concentrations at or before the beginning of rainstorms (low discharge). In this catchment, there is no flow in ground surface at no-rain days, but the discharge at the spring outlet occurs almost all the time.

During low-flow periods, most groundwater is retained in underground networks (Zhang et al., 2019) and has enough time to interact with carbonates, leading to the accumulation of solutes and products. At the early stage of rainstorms, rainwater infiltrates into epikarst initially and is intercepted in the aquifer (Williams, 2008), mixing with "old" water in soil or matrix. This process usually accompanies the dissolution of soil CO_2. As rainstorms go on, rainfall is enough to generate hillslope runoff and surface runoff, and "old" water is extruded and gradually replaced by the percolating "new" water. At this stage, the dominant pathway of underground flow is likely to change from matrix to conduit after saturating epikarst aquifer; the supplementary sources of solutes in spring can be quickly mobilized by the increasing discharge along pathways (Qin et al., 2020); the excess infiltration water would quickly pass through conduits and flow out at the outlet (Trček, 2007). This process can shorten the available time for both spring transportation and fluid-rock interaction (Tipper et al., 2006; Chen et al., 2018), generating differences on the transportation of both fluid and solutes (Bakalowicz, 2005; Bowes et al., 2005). Therefore, solute concentrations in SP decrease with increasing discharge and are gradually close to that in SU, and the effect of increasing discharge on solute concentrations is smaller in SU than SP. At the end of rainstorms, most available proximal sources near to or even within the flow pathways have been flushed. Hillslope runoff and surface runoff gradually decrease until they stop; spring runoff also decreases but normally maintains low discharge with slow velocity due to the recharge of matrix flow. Throughout the complete rainstorm, flow velocity, pathways, and the time for transportation and water-rock interaction all have been changing, leading to variations of sources and its contributions to solutes.

As highlighted by Thompson et al. (2011), the interpretation of $b \approx 0$ might be incomplete when the concentration variability is small. The ratio of CV of concentrations to CV of discharge (CV_C/CV_Q) is an alternative metric to statistically assess chemostatic behavior (Thompson et al., 2011; Musolff et al., 2015; Duncan et al., 2017; Zimmer et al., 2019), which could be calculated as follows:

$$\frac{CV_C}{CV_Q} = \frac{\mu_Q \sigma_C}{\mu_C \sigma_Q} \quad (3)$$

where μ and σ represent the mean and the standard deviation of concentrations (μ_C and σ_C) and discharge (μ_Q and σ_Q), respectively. The condition of $-0.2 < b < 0.2$ and $CV_C/CV_Q < 1$ is deemed a criterion of chemostatic behavior (Thompson et al., 2011; Zimmer et al., 2019). A $CV_C/CV_Q > 1$ indicates a relatively bigger variability in concentration than discharge,

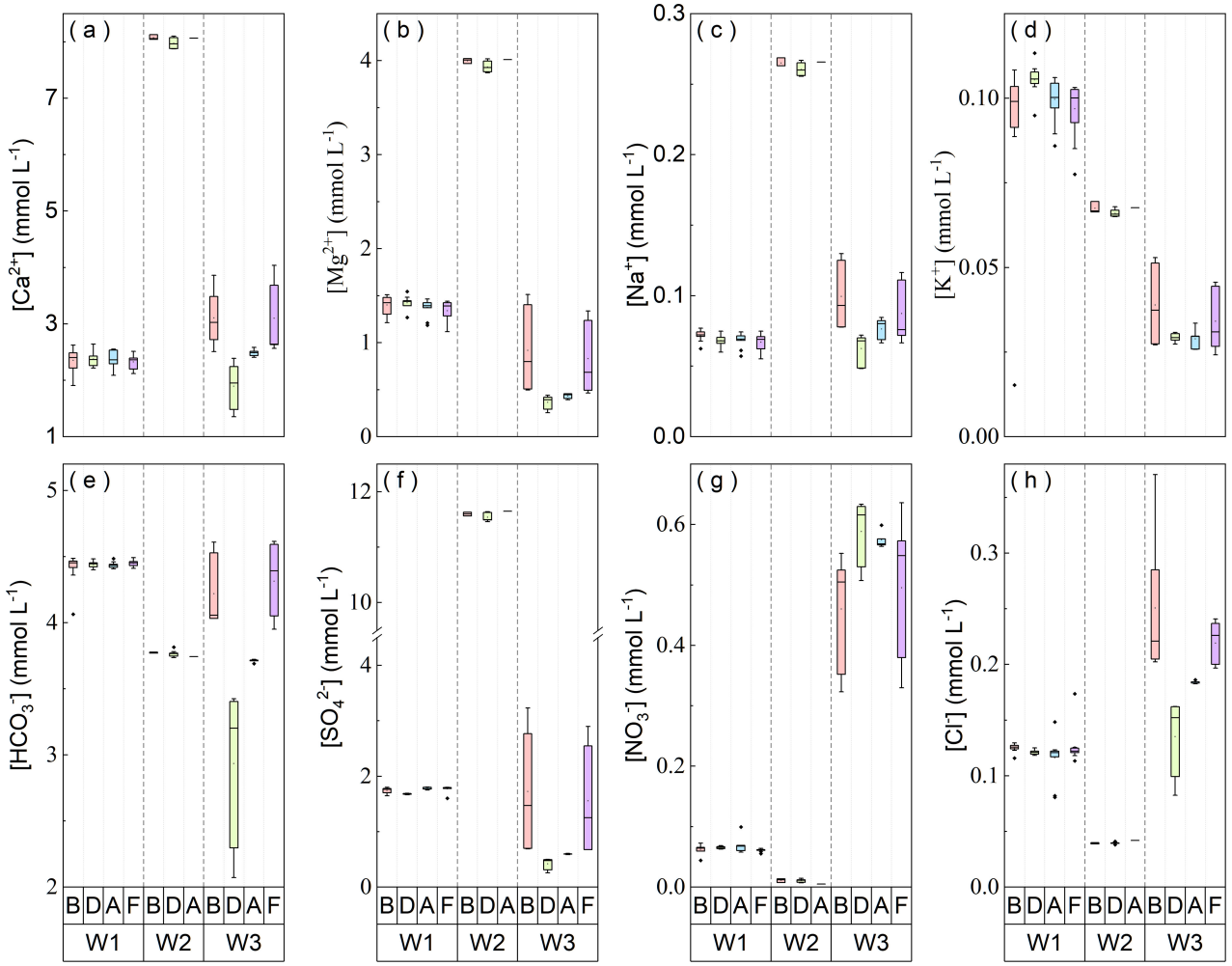

FIGURE 4 | The variation of ion concentrations in water collected from three observation wells before **(B)**, during **(D)**, after **(A)**, and on the fourth days **(F)** after the rainstorms. W1, W2, and W3 refer to three observation wells. Each box plot corresponds to an individual depth-profile.

which is usually referred to as "chemodynamic" (Musolff et al., 2015). According to the export regime classification system proposed by Musolff et al. (2015), plot of b vs. CV_C/CV_Q can be used to intuitively categorize and compare various solutes in catchment or between catchments (**Figure 6**). HCO_3^-, Ca^{2+}, and Mg^{2+} in both SU and SP have near-zero b values and low CV_C/CV_Q ratios ($<< 1$), indicating chemostatic behaviors. The three ions in Yu River (Liu J. et al., 2020) and Xijiang River (Zhong et al., 2018) display similar export regime with this study, but their chemostatic behaviors are relatively weaker. Conversely, there are scenes of $b > 0$ for the three ions in the Bode River of central Germany (Musolff et al., 2015) and Ca^{2+} in SU of Los Alamos (Koger et al., 2018), showing an enrichment trend. This phenomenon indicates their large potential supplements with increasing discharge. Other ions in this study display weaker chemostatic behavior, especially Na^+ and NO_3^- in SU and Na^+, SO_4^{2-} and NO_3^- in SP, implying that the pool of these ions is more susceptible to dilution, which is mainly due to their slower release or lower quantities along flowing pathways (Qin et al., 2020). SO_4^{2-} in SP is more sensitive to hydrological variation than that in SU. This is similar to the results from Los Alamos (Koger et al., 2018) and signifies that the potential sources of SO_4^{2-} in SP could be more quickly mobilized by increasing discharge. Overall, the dynamic response of hydrochemistry to rainstorms or climate change is largely controlled by regional hydrogeological properties (e.g., porosity, thickness, and hydraulic conductivity). It may differ between different conditions and needs to be analyzed using detailed local information. In this study, chemostatic is the predominant export regime of solutes in SU and SP.

During rainstorms, hydrochemistry in 3-wells respond differently to rainstorms, which is quicker in W3. This is mainly attributed to the higher permeability of epikarst around W3 (Chen et al., 2018). In the epikarst with better permeability, the relative proportion of vertical flow from infiltration replenishment increases and the lateral flow from "old" water

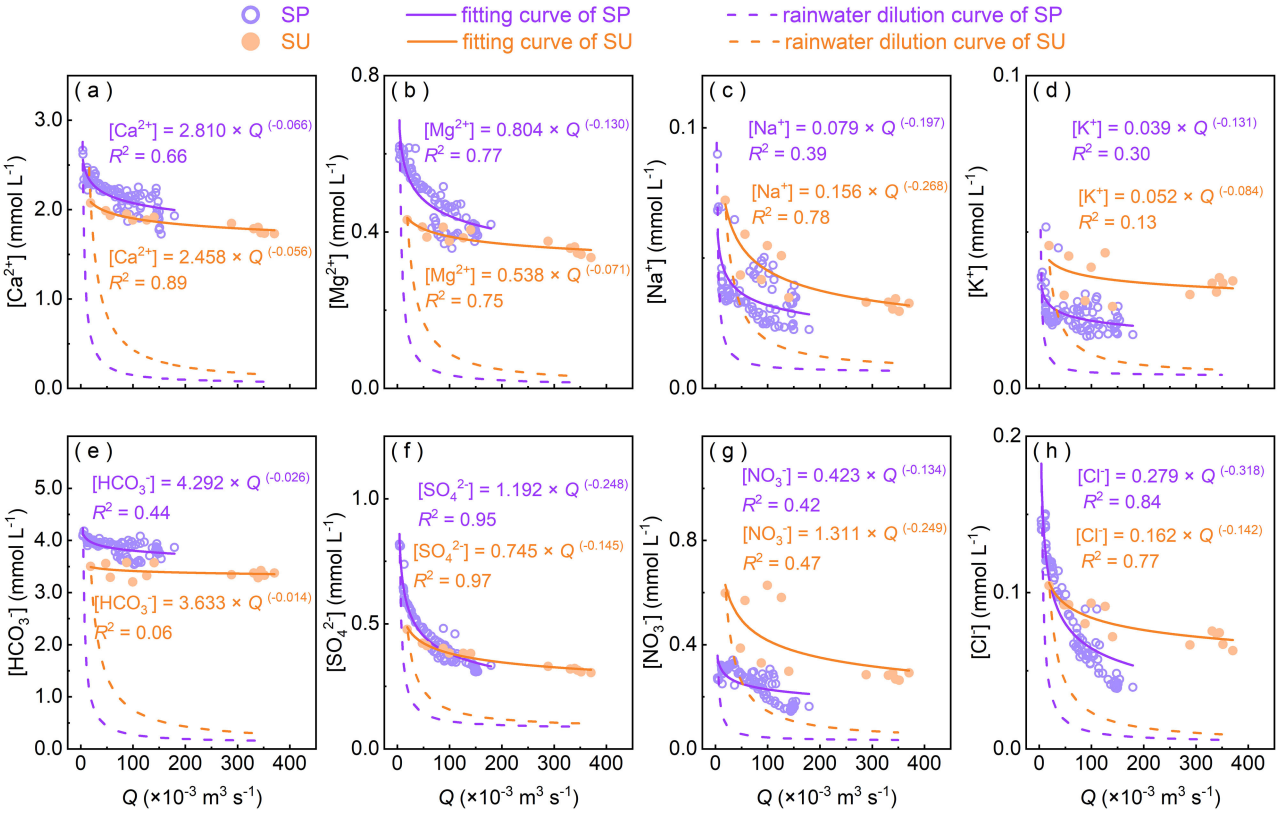

FIGURE 5 | Power-law relationships ($C = a\,Q^b$) between concentration (C) of major ions and discharge (Q). Rainwater dilution curves denote ideal conditions that ions are purely diluted by local rainwater. SU and SP refer to surface water and spring water, respectively.

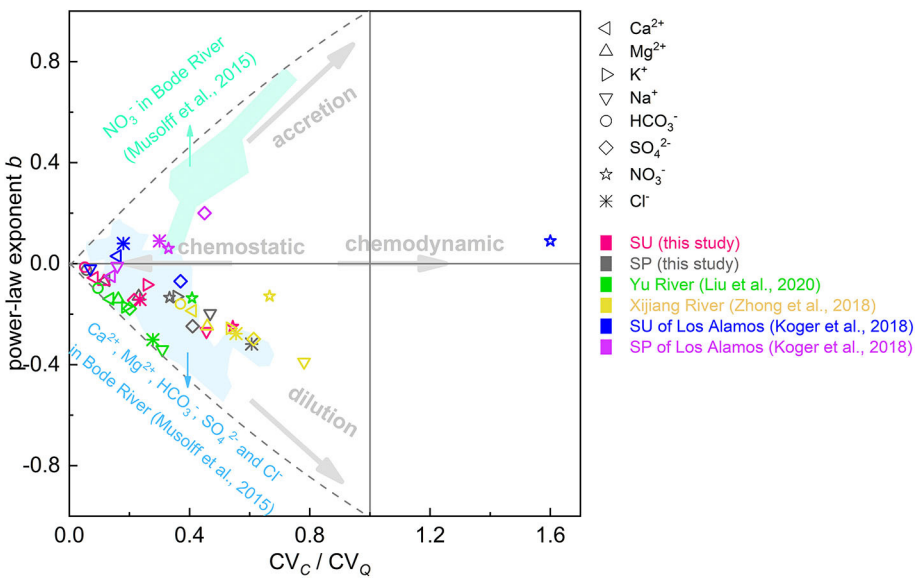

FIGURE 6 | Plot of b (the power-law exponent of $C=aQ^b$) vs. CV_C/CV_Q (the ratio of CV of concentrations to CV of discharge) for ions in different catchments. SU and SP refer to surface water and spring water, respectively. The shadow areas classify corresponding zones of ions in Bode River catchment (Musolff et al., 2015).

is gradually extruded out with the ongoing rainstorms (Zhang et al., 2019). At the second sampling (D), large inputting water in W3 diluted solute concentrations, excluding [NO_3^-], which may be affected by fertilizer application and some biological processes (Yue et al., 2020). The highest CV of [HCO_3^-] in W3 at this time is possibly caused by the variation of dissolved soil

CO_2 and soil respiration during infiltration processes (Qin et al., 2020). At the third sampling (A), the relative ratio of vertical flow to lateral flow might remain constant or infiltration water might dominate discharge, leading to small profile variation for solute concentrations in W3. At the fourth sampling (F), water level and chemistries in W3 nearly restored to the situation before the rainstorms. The permeability of epikarst normally weakens with increasing depth (Ford and Williams, 2007). W2 is a deep confined well fed by groundwater draining a gypsum stratum and not susceptible to changes in external environment (e.g., occurrences of rainstorms and agricultural activities) (Qin et al., 2019). Therefore, its hydrological environment is stable with smaller $[NO_3^-]$ and lower CV of most ions. $[SO_4^-]$ in W2 is approximately an order of magnitude higher than that in other 2-wells; $[Ca^{2+}]$ and $[Mg^{2+}]$ are also higher. It is thus reasonable to deduce the existence of gypsum dissolution and gypsum-induced dedolomitization around W2. Overall, the heterogeneous permeability of epikarst can affect the mixture of groundwater from different sources and flowing pathways, eventually enabling hydrochemistry in groundwater at different hydrogeological

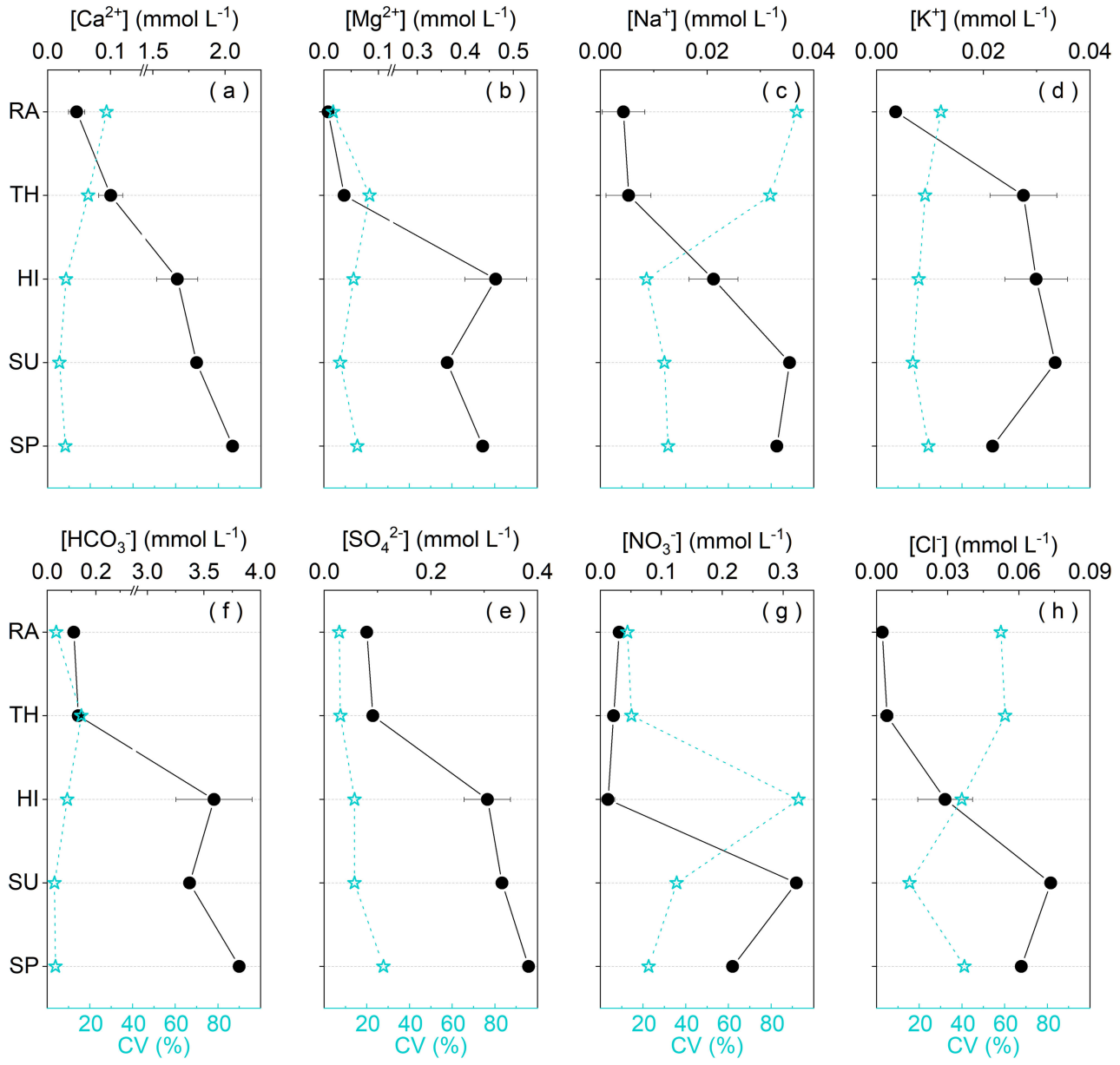

FIGURE 7 | The dynamic changes of ion concentrations among different spatial levels and corresponding CV during the rainstorms. In this figure, ion concentrations in rainwater (RA), throughfall (TH), and hillslope runoff (HI) are mean values with standard deviation. Discharge-weighted concentrations (DWC) are shown for surface water (SU) and spring (SP).

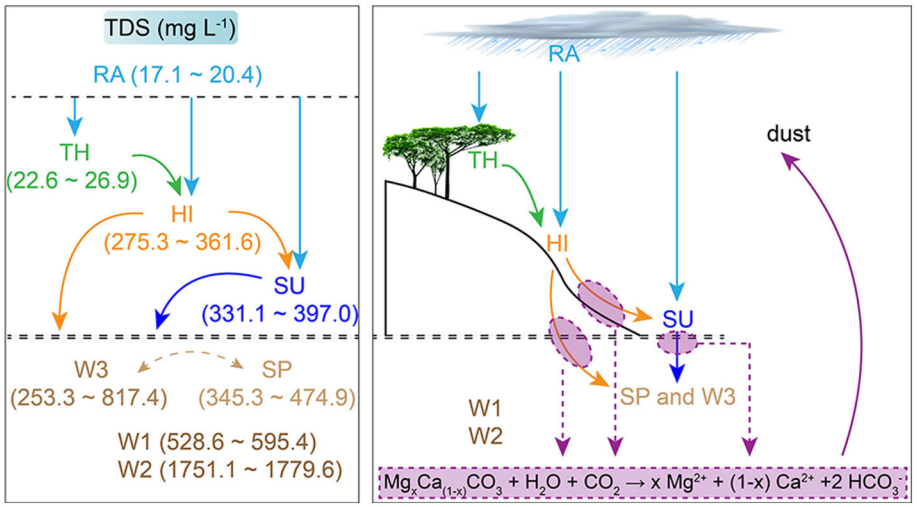

FIGURE 8 | Schematic diagram showing the possible transport processes of TDS and waters among different spatial levels.

conditions to display discrepant responses to rainstorms or discharge variations.

Dynamic Variations of Hydrochemistry Among Different Spatial Levels

The pH value of RA in this study is higher than that of other karst or forest regions in Southwest China, e.g., Guiyang of 4.5 (Han and Liu, 2006) and Chongqing of 4.75 (Ma et al., 2017), but it is lower than that of some areas in Northwestern China, e.g., Alxa Desert Plateau of 7.6 (Rao et al., 2017) and Urumqi River Valley of 7.0 (Zhao et al., 2008). This is most likely attributed to active carbon circulation and intense carbonate weathering within this karst depression (Qin et al., 2020). These processes can release some alkaline products (e.g., $CaCO_3$ and $MgCO_3$) into the atmosphere, neutralizing rainwater acidity (Tang and Han, 2019). [SO_4^{2-}] and [Ca^{2+}] in RA are much lower than that a decade ago (Wu et al., 2012), indicating that acid deposition has decreased after implementing environmental protection policies. This may also account for the higher pH in RA in this study than before. But [SO_4^{2-}] and [NO_3^-] in RA of this study are higher than that in Central Tibetan Plateau (Li et al., 2007), Eastern Tien Shan (Zhao et al., 2008), and Xisha Islands of South China Sea (Xiao et al., 2016), so there is still the possibility of anthropogenic emissions (NO_x, NH_3, and SO_x).

Migration processes of water among different spatial levels of Earth's Critical Zone can alter ion concentrations to different degrees (**Figure 7**). The variations of chemical compositions after passing through the vegetation canopy are mainly ascribed to (1) the adsorption of NO_3^- by vegetation (Polkowska et al., 2005); (2) the volatilization of HNO_3 after increasing its exposed area in vegetation surface; (3) the dissolution of $Ca^{2+}$and K^+ transported from roots to leaves through transpiration and respiration; and (4) the flushing of atmospheric particulates that contain ions (Ca^{2+}, Mg^{2+}, SO_4^{2-}, and K^+) and accumulate in vegetation surface during dry deposition. In karst regions, some weathering products could be released to ambient atmosphere with dust and pedogenesis processes (Lü et al., 2017). This possibly also affects $Ca^{2+}$and Mg^{2+} in RA and TH in this karst catchment, as demonstrated by **Supplementary Figure 2**. However, NH_4^+, one dominant ion in rainwater originating mainly from NH_3 emission of agricultural soil (Zeng et al., 2019), was not measured or considered when calculating TZ^+ and NICB in this study. This should be responsible for the imbalance of net inorganic charge. The better NICB in TH than in RA indirectly means that the vegetation canopy may intercept some NH_4^+ from RA. All these hydrochemical variations above are also the causes of the elevation of pH in TH relative to RA. Solutes in rivers are mostly derived from rock weathering, atmosphere, and anthropogenic inputs (Gaillardet et al., 1999; Qin et al., 2019). In this study, most solute concentrations in SU and SP are much higher than that in RA and TH (**Figure 7**), indicating little contributions of atmospheric sources compared with terrestrial sources. Carbonate weathering is one major source for this catchment (**Supplementary Figure 2**). [Ca^{2+}], [Mg^{2+}], and [HCO_3^-] in HI are far higher than that in RA and TH but closer to that in SU and SP (**Figure 7**), indicating that the contribution of carbonate weathering and CO_2 dissolution may already exist when hillslope runoff occurs. Their relative contribution ratios are different from that generated during surface and underground processes, as illustrated in **Figure 8**. Additionally, [Ca^{2+}], [Mg^{2+}], and [HCO_3^-] in SP are higher than that in SU (**Figure 7**). One possible explanation is that during the infiltration of flow through epikarst and the spring transportation within an underground conduit, there is dissolution of more soil CO_2 and intense carbonate weathering (Qin et al., 2020). In this agricultural karst depression, NO_3^- characterizes nitrification and owns large input from reductive nitrogen fertilizer and manure (Yue et al., 2020). Cl^- is deemed to have similar source area or transport pathways with NO_3^- (Qin et al., 2020). K^+ can also accumulate in soil surface after the application of potash fertilizer due to cation exchange and relative high contents in biomass (Boy et al., 2008). Therefore, NO_3^-, Cl^-, and K^+ all have potential

TABLE 1 | Varimax rotated component matrix for physic-chemical parameters in water at different spatial levels.

Parameters	PC1	PC2	PC3	PC4	Extraction
Ca^{2+}	0.992				0.709
Na^{+}	0.970				0.995
SO_4^{2-}	0.969				0.829
EC	0.963				0.909
Mg^{2+}	0.927				0.992
K^{+}		0.887			0.932
T		0.815			0.996
DO		−0.808			0.975
NO_3^-			0.885		0.906
Cl^-			0.854		0.915
pH				0.896	0.990
HCO_3^-				0.797	0.872
Eigenvalues	5.087	2.666	1.746	1.552	
Variance (%)	42.394	22.215	14.551	12.935	
Cumulative (%)	42.394	64.609	79.160	92.095	

Extraction method, principal component analysis; Rotation method, Varimax with Kaiser normalization. Here we only show loadings with high scores (>0.7).

agricultural sources and might be intercepted by epikarst during infiltration processes, leading to lower concentrations in SP than in SU (**Figure 7**). Overall, the difference of hydrochemistry among different water bodies is related to the double properties of agriculture and karst in this depression catchment.

In order to acquire descriptive statistics and explore interactive effects among physic-chemical parameters, principle component analysis (PCA) was performed with varimax rotation. The Kaiser-Meyer-Olkin (KMO) Measure of Sampling Adequacy and Bartlett's Test of Sphericity were conducted and generated a value of 0.738 with the significance of <0.001, indicating the suitability of the dataset for PCA. As shown in **Table 1**, there are four components (PC, eigenvalues >1), totally explaining 92.095% of the variation. PC1 explains 42.394% of the total variance and has high positive loading values (>0.9) of Ca^{2+}, Na^{+}, SO_4^{2-}, EC, and Mg^{2+}. This indicates that these parameters may follow an alike trend that is possibly due to same controls or sources areas or transit pathways. According to the common properties of these parameters, PC1 could be attributed to geological origins. This also indirectly reflects that EC is mainly controlled by Ca^{2+}, Mg^{2+}, and SO_4^{2-}. The main geological source of SO_4^{2-} is gypsum dissolution. PC2 can explain 18.56% of the total variance and includes two positive loadings (K^{+} and T) and one negative loading (DO), indicating that temperature and dissolved oxygen may exert positive and negative influences on the eluviation of K^{+}, respectively. PC2 could be partially attributed to the influence of the mixing of soil and natural factors. NO_3^- and Cl^- are two positive loadings of PC3 that can explain 14.551% of the variance and is likely to denote agricultural contributions. Additionally, PC4 can only explain 12.935% variance by pH and HCO_3^-, and HCO_3^- owns a loading of <0.8. Because HCO_3^- is mostly contributed by soil CO_2 that is controlled by respiration and microbiologic activities (Qin et al., 2020), we conclude that PC4 is mainly contributed by biological sources.

Despite the differences of hydrochemical concentrations and controlling factors among different spatial levels, all waters show the dominance of HCO_3^- and Ca^{2+} in ions (except W2 draining a gypsum stratum) (**Supplementary Figure 3**), reflecting the characteristics of karst water. It is worth noting that Chenqi catchment has continual agricultural activities (e.g., fertilization and herding), so topsoil can store or accumulate NO_3^- and Cl^-. As a rainstorm occurs, water head of groundwater varies with hydrology, regulating nutrient exchange between matrix flow and conduit flow. Because the transportation from conduits to matrix is faster than that from matrix to conduits (Li et al., 2008), there is potential chronic pollution on karst groundwater in this agricultural catchment. Additionally, the accumulation of Ca^{2+} and Mg^{2+} in karst groundwater can elevate hardness of water. Both can deteriorate regional water quality during a certain period.

CONCLUSIONS

Rainwater, throughfall, hillslope runoff, surface water, spring, and well water at different hydrogeological conditions were collected synchronously during rainstorms to analyze the dynamic responses of hydrochemistry and its variation at different spatial levels at a karst Critical Zone Observatory (CZO), Southwest China. In this karst depression, pH and TDS in rainwater are 6.71 ± 0.03 and 18.6 ± 1.17 mg L^{-1}, respectively. After passing through the vegetation canopy, pH increases by 0.4, and most ion concentrations also have increments with different degrees (except [NO_3^-] which decreases by 4.1–54.0%). Chemical compositions in rainwater and throughfall could be affected by both anthropogenic emission (NO_x, NH_3, and SO_x) and some weathering products (Ca^{2+} and Mg^{2+}) released to ambient atmosphere with dust. Wet deposition generally contributes little to hydrochemistry in surface water and groundwater. The influences of CO_2 dissolution and carbonate weathering on hydrochemistry already exist when hillslope runoff occurs, but their relative contribution ratios are different from that generated during surface and underground processes. Throughout the whole rainstorms, TDS in surface water and spring are 331–397 mg L^{-1} and 345–475 mg L^{-1}. Hydrochemistry in surface water and spring displays chemostatic responses with different intensities to discharge variations, possibly controlling by available sources and the difference between solute concentrations before and after rainstorms. Carbonate weathering contributes most to Ca^{2+} and Mg^{2+}, gypsum dissolution and gypsum-induced dedolomitization also regulate Ca^{2+}, Mg^{2+}, and SO_4^{2-} in deep confined well water draining a gypsum stratum. Soil CO_2 from respiration and microbiologic activities is one biological source of HCO_3^-. Agricultural activities are responsible for the chemostatic behavior of NO_3^-, Cl^-, and K^{+}, especially in surface water. All these were further demonstrated by principle component analysis (PCA). Epikarst aquifer with low permeability is insensitive to changes in external environment (e.g., occurrences of rainstorms

and agricultural activities). High permeability can enhance the response of epikarst aquifer to hydrological variations, deteriorating regional water quality (potential chronic pollution of nitrogen and high hardness of water) during a certain period. Optimal measures of water protection are necessary in agricultural karst catchment.

DATA AVAILABILITY STATEMENT

The original contributions presented in the study are included in the article/**Supplementary Materials**, further inquiries can be directed to the corresponding author/s.

AUTHOR CONTRIBUTIONS

CQ, S-LL, HD, and F-JY designed the research objectives and interpreted the data and prepared the manuscript. CQ, Z-JW, and JZ carried out the field and laboratory work. All authors discussed the results and commented on the manuscript.

FUNDING

This study was jointly funded by the National Key R&D Program of China (grant number 2016YFA0601002) and the National Natural Science Foundation of China (grant numbers 41571130072 and 41861144026).

ACKNOWLEDGMENTS

We thank Susan Waldron and Xi Chen for their discussions and suggestions. We also thank Sen Xu, Yu-Chong Fu, teachers in Puding Karst Ecosystem Observation and Research Station for their help in sensor installation and data collection.

SUPPLEMENTARY MATERIAL

The Supplementary Material for this article can be found online at: https://www.frontiersin.org/articles/10.3389/frwa.2020.577511/full#supplementary-material

REFERENCES

Ackerer, J., Steefel, C., Liu, F., Bart, R., Safeeq, M., O'Geen, A., et al. (2020). Determining how critical zone structure constrains hydrogeochemical behavior of watersheds: learning from an elevation gradient in California's Sierra Nevada. *Front. Water* 2:23. doi: 10.3389/frwa.2020.00023

Bakalowicz, M. (2005). Karst groundwater: a challenge for new resources. *Hydrogeol. J.* 13, 148–160. doi: 10.1007/s10040-004-0402-9

Basu, N. B., Destouni, G., Jawitz, J. W., Thompson, S. E., Loukinova, N. V., Darracq, A., et al. (2010). Nutrient loads exported from managed catchments reveal emergent biogeochemical stationarity. *Geophys. Res. Lett.* 37:L23404. doi: 10.1029/2010GL045168

Beaulieu, E., Goddéris, Y., Donnadieu, Y., Labat, D., and Roelandt, C. (2012). High sensitivity of the continental-weathering carbon dioxide sink to future climate change. *Nat. Clim. Change* 2, 346–349. doi: 10.1038/nclimate1419

Bowes, M. J., House, W. A., Hodgkinson, R. A., and Leach, D. V. (2005). Phosphorus-discharge hysteresis during storm events along a river catchment: the River Swale, UK. *Water Res.* 39, 751–762. doi: 10.1016/j.watres.2004.11.027

Boy, J., Valarezo, C., and Wilcke, W. (2008). Water flow paths in soil control element exports in an Andean tropical montane forest. *Eur. J. Soil Sci.* 59, 1209–1227. doi: 10.1111/j.1365-2389.2008.01063.x

Chen, H. Y., Chen, B. Y., and Chen, B. (2005). Lithologic characteristics of Houzhai karst small valley, Puding, Guizhou Province. *Guizhou Geol.* 22, 284–288 (in Chinese).

Chen, X., Zhang, Z., Soulsby, C., Cheng, Q., Binley, A., Jiang, R., et al. (2018). Characterizing the heterogeneity of karst critical zone and its hydrological function: an integrated approach. *Hydrol. Process.* 32, 2932–2946. doi: 10.1002/hyp.13232

Cheng, Q., Chen, X., Tao, M., and Binley, A. (2019). Characterization of karst structures using quasi-3D electrical resistivity tomography. *Environ. Earth Sci.* 78:285. doi: 10.1007/s12665-019-8284-2

Clow, D. W., and Mast, M. A. (2010). Mechanisms for chemostatic behavior in catchments: Implications for CO_2 consumption by mineral weathering. *Chem. Geol.* 269, 40–51. doi: 10.1016/j.chemgeo.2009.09.014

Correa, A., Breuer, L., Crespo, P., Celleri, R., Feyen, J., Birkel, C., et al. (2019). Spatially distributed hydro-chemical data with temporally high-resolution is needed to adequately assess the hydrological functioning of headwater catchments. *Sci. Total Environ.* 651, 1613–1626. doi: 10.1016/j.scitotenv.2018.09.189

Duncan, J. M., Welty, C., Kemper, J. T., Groffman, P. M., and Band, L. E. (2017). Dynamics of nitrate concentration-discharge patterns in an urban watershed. *Water Resour. Res.* 53, 7349–7365. doi: 10.1002/2017WR020500

Ford, D., and Williams, P. (2007). *Karst Hydrogeology and Geomorphology*. Chichester: John Wiley & Sons.

Gabet, E. J., Edelman, R., and Langner, H. (2006). Hydrological controls on chemical weathering rates at the soil-bedrock interface. *Geology* 34, 1065–1068. doi: 10.1130/G23085A.1

Gaillardet, J., Dupre, B., Louvat, P., and Allegre, C. J. (1999). Global silicate weathering and CO_2 consumption rates deduced from the chemistry of large rivers. *Chem. Geol.* 159, 3–30. doi: 10.1016/S0009-2541(99)00031-5

Godsey, S. E., Kirchner, J. W., and Clow, D. W. (2009). Concentration-discharge relationships reflect chemostatic characteristics of US catchments. *Hydrol. Process.* 23, 1844–1864. doi: 10.1002/hyp.7315

Han, G., and Liu, C.-Q. (2004). Water geochemistry controlled by carbonate dissolution: a study of the river waters draining karst-dominated terrain, Guizhou Province, China. *Chem. Geol.* 204, 1–21. doi: 10.1016/j.chemgeo.2003.09.009

Han, G., and Liu, C. Q. (2006). Strontium isotope and major ion chemistry of the rainwaters from Guiyang, Guizhou Province, China. *Sci. Total Environ.* 364, 165–174. doi: 10.1016/j.scitotenv.2005.06.025

Kačaroglu, F. (1999). Review of groundwater pollution and protection in karst areas. *Water Air Soil Pollut.* 113, 337–356. doi: 10.1023/A:1005014532330

Koger, J. M., Newman, B. D., and Goering, T. J. (2018). Chemostatic behaviour of major ions and contaminants in a semiarid spring and stream system near Los Alamos, NM, USA. *Hydrol. Process.* 32, 1709–1716. doi: 10.1002/hyp.11624

Lang, Y.-C., Liu, C.-Q., Zhao, Z.-Q., Li, S.-L., and Han, G.-L. (2006). Geochemistry of surface and ground water in Guiyang, China: water/rock interaction and pollution in a karst hydrological system. *Appl. Geochem.* 21, 887–903. doi: 10.1016/j.apgeochem.2006.03.005

Li, C., Kang, S., Zhang, Q., and Kaspari, S. (2007). Major ionic composition of precipitation in the Nam Co region, Central Tibetan Plateau. *Atmos. Res.* 85, 351–360. doi: 10.1016/j.atmosres.2007.02.006

Li, G. Q., Loper, D. E., and Kung, R. (2008). Contaminant sequestration in karstic aquifers: experiments and quantification. *Water Resour. Res.* 44:W02429. doi: 10.1029/2006WR005797

Liu, J., Zhong, J., Ding, H., Yue, F. J., Li, C., Xu, S., et al. (2020). Hydrological regulation of chemical weathering and dissolved inorganic carbon biogeochemical processes in a monsoonal river. *Hydrol. Process.* 34, 2780–2792. doi: 10.1002/hyp.13763

Liu, M., Han, G., and Zhang, Q. (2020). Effects of agricultural abandonment on soil aggregation, soil organic carbon storage and stabilization: Results from observation in a small karst catchment, Southwest China. *Agric. Ecosyst. Environ.* 288:106719. doi: 10.1016/j.agee.2019.106719

Lü, P., Han, G., and Wu, Q. (2017). Chemical characteristics of rainwater in karst rural areas, Guizhou Province, Southwest China. *Acta Geochim.* 36, 572–576. doi: 10.1007/s11631-017-0238-3

Lu, X., Li, L. Y., Li, N., Yang, G., Luo, D., and Chen, J. (2011). Chemical characteristics of spring rainwater of Xi'an city, NW China. *Atmos. Environ.* 45, 5058–5063. doi: 10.1016/j.atmosenv.2011.06.026

Ma, M., Sun, T., Li, D. K., and Wang, D. Y. (2017). Dynamics of the water quality in a broad-leaf evergreen forest at different spatial levels on Jinyun mountain. *Environ. Sci.* 38, 5056–5062. doi: 10.13227/j.hjkx.201704208

Musolff, A., Schmidt, C., Selle, B., and Fleckenstein, J. H. (2015). Catchment controls on solute export. *Adv. Water Resourc.* 86, 133–146. doi: 10.1016/j.advwatres.2015.09.026

Piazza, G. A., Dupas, R., Gascuel-Odoux, C., Grimaldi, C., Pinheiro, A., and Kaufmann, V. (2018). Influence of hydroclimatic variations on solute concentration dynamics in nested subtropical catchments with heterogeneous landscapes. *Sci. Total Environ.* 635, 1091–1101. doi: 10.1016/j.scitotenv.2018.03.394

Polkowska, Z., Astel, A., Walna, B., Małek, S., Medrzycka, K., Górecki, T., et al. (2005). Chemometric analysis of rainwater and throughfall at several sites in Poland. *Atmos. Environ.* 39, 837–855. doi: 10.1016/j.atmosenv.2004.10.026

Qin, C., Li, S.-L., Waldron, S., Yue, F.-J., Wang, Z.-J., Zhong, J., et al. (2020). High-frequency monitoring reveals how hydrochemistry and dissolved carbon respond to rainstorms at a karstic critical zone, Southwestern China. *Sci. Total Environ.* 714:136833. doi: 10.1016/j.scitotenv.2020.136833

Qin, C., Li, S. L., Yue, F. J., Xu, S., and Ding, H. (2019). Spatiotemporal variations of dissolved inorganic carbon and controlling factors in a small karstic catchment, Southwestern China. *Earth Surf. Process. Landf.* 44, 2423–2436. doi: 10.1002/esp.4672

Rao, W., Han, G., Tan, H., Jin, K., Wang, S., and Chen, T. (2017). Chemical and Sr isotopic characteristics of rainwater on the Alxa Desert Plateau, North China: implication for air quality and ion sources. *Atmos. Res.* 193, 163–172. doi: 10.1016/j.atmosres.2017.04.007

Tang, Y., and Han, G. (2019). Seasonal variation and quality assessment of the major and trace elements of atmospheric dust in a typical karst city, Southwest China. *Int. J. Environ. Res. Public Health* 16:325. doi: 10.3390/ijerph16030325

Thompson, S. E., Basu, N. B., Lascurain, J. Jr., Aubeneau, A., and Rao, P. S. C. (2011). Relative dominance of hydrologic versus biogeochemical factors on solute export across impact gradients. *Water Resour. Res.* 47:WOOJ05. doi: 10.1029/2010WR009605

Tipper, E. T., Bickle, M. J., Galy, A., West, A. J., Pomies, C., and Chapman, H. J. (2006). The short term climatic sensitivity of carbonate and silicate weathering fluxes: insight from seasonal variations in river chemistry. *Geochim. Cosmochim. Acta* 70, 2737–2754. doi: 10.1016/j.gca.2006.03.005

Trček, B. (2007). How can the epikarst zone influence the karst aquifer hydraulic behaviour? *Environ. Geol.* 51, 761–765. doi: 10.1007/s00254-006-0387-x

Williams, P. W. (2008). The role of the epikarst in karst and cave hydrogeology: a review. *Int. J. Speleol.* 37, 1–10. doi: 10.5038/1827-806X.37.1.1

Wu, Q., Han, G., Tao, F., and Tang, Y. (2012). Chemical composition of rainwater in a karstic agricultural area, Southwest China: the impact of urbanization. *Atmos. Res.* 111, 71–78. doi: 10.1016/j.atmosres.2012.03.002

Xiao, H., Xiao, H., Zhang, Z., Wang, Y., Long, A., and Liu, C. (2016). Chemical characteristics and source apportionment of atmospheric precipitation in Yongxing Island. *China Environ. Sci.* 36, 3237–3244 (in Chinese).

Yuan, D., and Cai, G. (1988). *The Science of Karst Environment*. Chongqing: Chongqing Publishers. p. 1–332 (in Chinese).

Yuan, D., and Zhang, C. (2008). Karst dynamics theory in China and its practice. *Acta Geosci. Sin.* 29, 355–365 (in Chinese).

Yue, F. J., Li, S. L., Waldron, S., Wang, Z. J., Oliver, D. M., Chen, X., et al. (2020). Rainfall and conduit drainage combine to accelerate nitrate loss from a karst agroecosystem: Insights from stable isotope tracing and high-frequency nitrate sensing. *Water Res.* 186:116388. doi: 10.1016/j.watres.2020.116388

Zeng, J., Yue, F.-J., Wang, Z.-J., Wu, Q., Qin, C.-Q., and Li, S.-L. (2019). Quantifying depression trapping effect on rainwater chemical composition during the rainy season in karst agricultural area, southwestern China. *Atmos. Environ.* 218:116998. doi: 10.1016/j.atmosenv.2019.116998

Zhang, X., Jiang, H., Zhang, Q., and Zhang, X. (2012). Chemical characteristics of rainwater in northeast China, a case study of Dalian. *Atmos. Res.* 116, 151–160. doi: 10.1016/j.atmosres.2012.03.014

Zhang, Z., Chen, X., Cheng, Q., and Soulsby, C. (2019). Storage dynamics, hydrological connectivity and flux ages in a karst catchment: conceptual modelling using stable isotopes. *Hydrol. Earth Syst. Sci.* 23, 51–71. doi: 10.5194/hess-23-51-2019

Zhao, D., and Seip, H. M. (1991). Assessing effects of acid deposition in Southwestern China using the magic model. *Water Air Soil Pollut.* 60, 83–97. doi: 10.1007/BF00293967

Zhao, Z., Tian, L., Fischer, E., Li, Z., and Jiao, K. (2008). Study of chemical composition of precipitation at an alpine site and a rural site in the Urumqi River Valley, Eastern Tien Shan, China. *Atmos. Environ.* 42, 8934–8942. doi: 10.1016/j.atmosenv.2008.08.003

Zhong, J., Li, S. L., Ibarra, D. E., Ding, H., and Liu, C. Q. (2020). Solute production and transport processes in Chinese monsoonal rivers: implications for global climate change. *Global Biogeochem. Cycles* 34:e2020GB006541. doi: 10.1029/2020GB006541

Zhong, J., Li, S. L., Liu, J., Ding, H., Sun, X. L., Xu, S., et al. (2018). Climate variability controls on CO_2 consumption fluxes and carbon dynamics for monsoonal rivers: evidence from Xijiang river, Southwest China. *J. Geophys. Rese. Biogeosci.* 123, 2553–2567. doi: 10.1029/2018JG004439

Zhou, X., Xu, Z., Liu, W., Wu, Y., Zhao, T., Jiang, H., et al. (2019). Chemical composition of precipitation in Shenzhen, a coastal mega-city in South China: influence of urbanization and anthropogenic activities on acidity and ionic composition. *Sci. Total Environ.* 662, 218–226. doi: 10.1016/j.scitotenv.2019.01.096

Zimmer, M. A., Pellerin, B., Burns, D. A., and Petrochenkov, G. (2019). Temporal variability in nitrate-discharge relationships in large rivers as revealed by high-frequency data. *Water Resour. Res.* 55, 973–989. doi: 10.1029/2018WR023478

Conflict of Interest: The authors declare that the research was conducted in the absence of any commercial or financial relationships that could be construed as a potential conflict of interest.